ACS Energy LETTERS

http://pubs.acs.org/journal/aelccp

A 2.6 m Aqueous Electrolyte for High-Energy-Density Lithium-Ion Pouch Cells Using NbO_2 Anode

Published as part of ACS Energy Letters special issue "The Evolving Landscape of Energy Research: Insights from Leading Researchers".

Chuanyu Hou, Changming Ke, Runze Chen, Yangfan Lin, Qin Huang, Shi Liu,* and Jianhui Wang*

Cite This: ACS Energy Lett. 2026, 11, 654−663

Read Online

ACCESS | Metrics & More | Article Recommendations | Supporting Information

ABSTRACT: Niobium-based oxides are promising high-energy-density anodes (>300 mAh g^{-1} at 1.0−2.0 V vs Li^+/Li) but face challenges with conventional aqueous electrolytes. Herein, we develop a cost-effective, dilute aqueous electrolyte modulated by methylurea (MU), a nonflammable, low-toxicity cosolvent. Leveraging its donor−acceptor amphiphilicity and structural asymmetry, MU enhances miscibility with salt and water, enabling a 2.6 m solution with a distinctive solvation structure: an inner sheath dominated by MU and anions, and an outer layer where water is anchored by MU. This configuration reduces water activity and promotes a robust organic−inorganic interphase, effectively suppressing hydrogen evolution and extending the cathodic stability limit to 1.2 V vs Li^+/Li. Pouch cells of $NbO_2|LiCoO_2$ and $NbO_2|LiMn_2O_4$ show 96% capacity retention after 24 h at 100% state of charge, along with stable cycling over 150 cycles at 0.25 C. This strategy enhances aqueous battery performance while maintaining safety and cost-efficiency, advancing practical implementation.

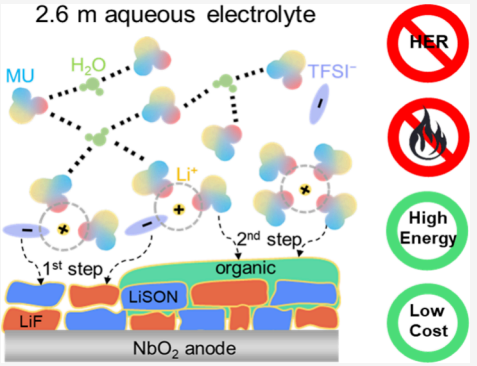

Driven by the rapid growth of electric vehicles and large-scale energy storage, lithium-ion batteries require continuous advancements in performance and safety.[1] However, commercial nonaqueous lithium-ion electrolytes are flammable, volatile, and toxic, posing serious safety risks.[2,3] Furthermore, their extreme sensitivity to moisture demands manufacturing in costly, energy-intensive dry-room environments. These limitations highlight the urgent need for safer and more cost-effective battery technologies. Aqueous batteries represent a promising alternative, with inherent advantages such as nonflammability, low toxicity, and simplified production.[4−7] Nevertheless, their progress is hindered by the narrow electrochemical stability window of water, which triggers parasitic hydrogen evolution reactions at low potentials. This fundamental constraint restricts the use of high-specific-capacity anode materials and limits the achievable cell voltage.[8,9] Consequently, the energy density of aqueous batteries remains less than one-third of that of nonaqueous lithium-ion batteries, significantly hindering their commercial competitiveness.

Niobium-based oxides are promising anode materials, owing to their three-dimensional tunnel structures and multielectron transfer capability.[10,11] Compared with commonly studied anode materials for aqueous batteries, such as $LiTi_2(PO_4)_3$ (138 mAh g^{-1}, 2.48 V vs Li^+/Li),[12] Mo_6S_8 (128 mAh g^{-1}, 2.80−2.20 V vs Li^+/Li),[4] anatase TiO_2 (168 mAh g^{-1}, 2.0−1.7 V vs Li^+/Li),[13] and $Li_4Ti_5O_{12}$ (175 mAh g^{-1}, 1.55 V vs Li^+/Li),[14,15] niobium-based oxides exhibit low lithium intercalation potentials (2.0−1.0 V vs Li^+/Li) and exceptionally high theoretical specific capacities (>300 mAh g^{-1}). However, this low operating potential also presents a severe challenge for aqueous electrolytes, as it falls outside water's narrow electrochemical stability window. Early studies utilized 21 m LiTFSI in H_2O electrolytes, but the limited cathodic stability (1.9 V vs Li^+/Li) restricted the usable capacity to below 80 mAh g^{-1}.[16] To improve the performance, dual-salt and ionic liquid systems were introduced to increase the salt concentration (e.g., 50 m LiTFSI + 30 m TMBTFSI in

Received: October 14, 2025
Revised: November 20, 2025
Accepted: December 5, 2025
Published: December 12, 2025

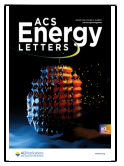

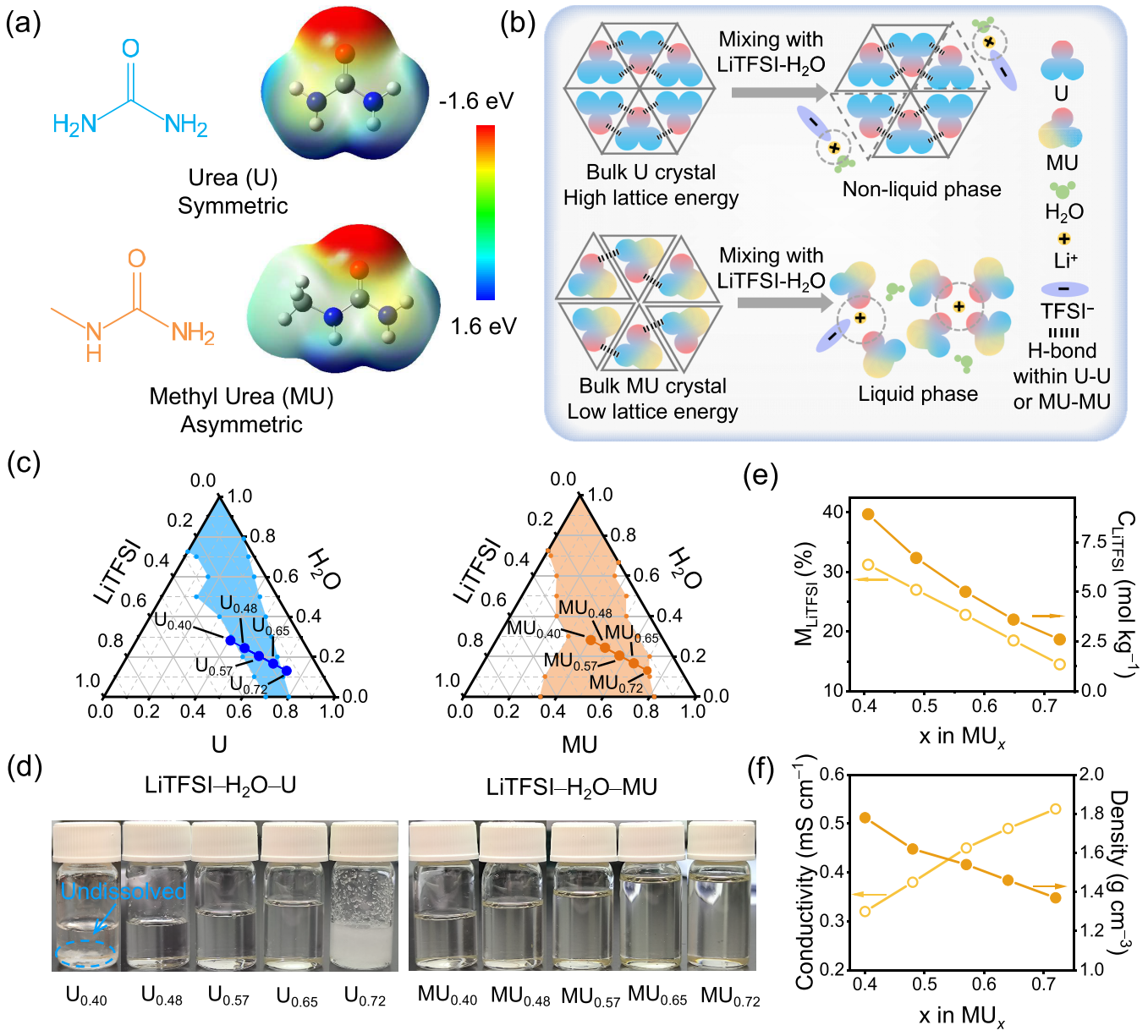

Figure 1. Design and characterization of a low-concentration MU-based aqueous electrolyte. (a) Molecular structures and electrostatic potential (ESP) of U and MU. (b) Schematic illustration of dissolution process for LiTFSI–H_2O–U and LiTFSI–H_2O–MU ternary systems. The symmetric U molecules form a stable, difficult-to-dissolve crystal, while the asymmetric MU molecules pack loosely, enabling facile dissolution and ion solvation. (c) Ternary phase diagrams for LiTFSI–H_2O–U and LiTFSI–H_2O–MU systems based on over 80 samples, showing the significantly broader liquid-phase achieved with MU. (d) Photographs of various electrolytes of U_x and MU_x (x is the molar fraction of U or MU in ternary systems). Both high and low salt-concentration U-based systems ($U_{0.40}$ and $U_{0.72}$) become immiscible, whereas MU-based systems remain homogeneous. (e) Mole fraction (M_{LiTFSI}) and concentration (C_{LiTFSI}) of LiTFSI in different electrolytes of MU_x, demonstrating the ability to drastically reduce salt concentration. (f) Key physicochemical properties, including ionic conductivity and density, for the series of MU_x electrolytes.

H_2O,[17] 40 m LiTFSI + 20 m EMITFSI in H_2O[18]), extending the cathodic stability and raising the usable capacity to 200 mAh g^{-1}. However, these strategies did not demonstrate a compelling performance advantage over that of the $Li_4Ti_5O_{12}$ electrode. Moreover, the marginal improvements came at the expense of significantly increased cost, as the use of ultrahigh concentrations of expensive fluorosulfonyl imide salts and/or ionic liquids undermined the fundamental economic benefits of aqueous systems. Despite these efforts, core challenges such as severe self-discharge and capacity degradation remain unresolved, particularly under practical low-rate cycling conditions, highlighting the persistent issue of parasitic reactions.

To overcome the trade-offs associated with salt-concentrated aqueous electrolytes, we build upon our prior work on a methylurea (MU)-regulated aqueous electrolyte, which features a core–shell solution structure with localized ultrahigh LiTFSI concentration enabled by interactions between MU, LiTFSI, and H_2O.[19] This system achieved a cathodic stability limit of 1.0 V vs Li^+/Li and supported stable cycling of high-energy-density rocking-chair NbO_2|$LiMn_2O_4$ full cells (175 Wh $kg^{-1}_{cathode+anode}$). While our previous 15.9 m electrolyte

https://doi.org/10.1021/acsenergylett.5c03327
ACS Energy Lett. 2026, 11, 654−663

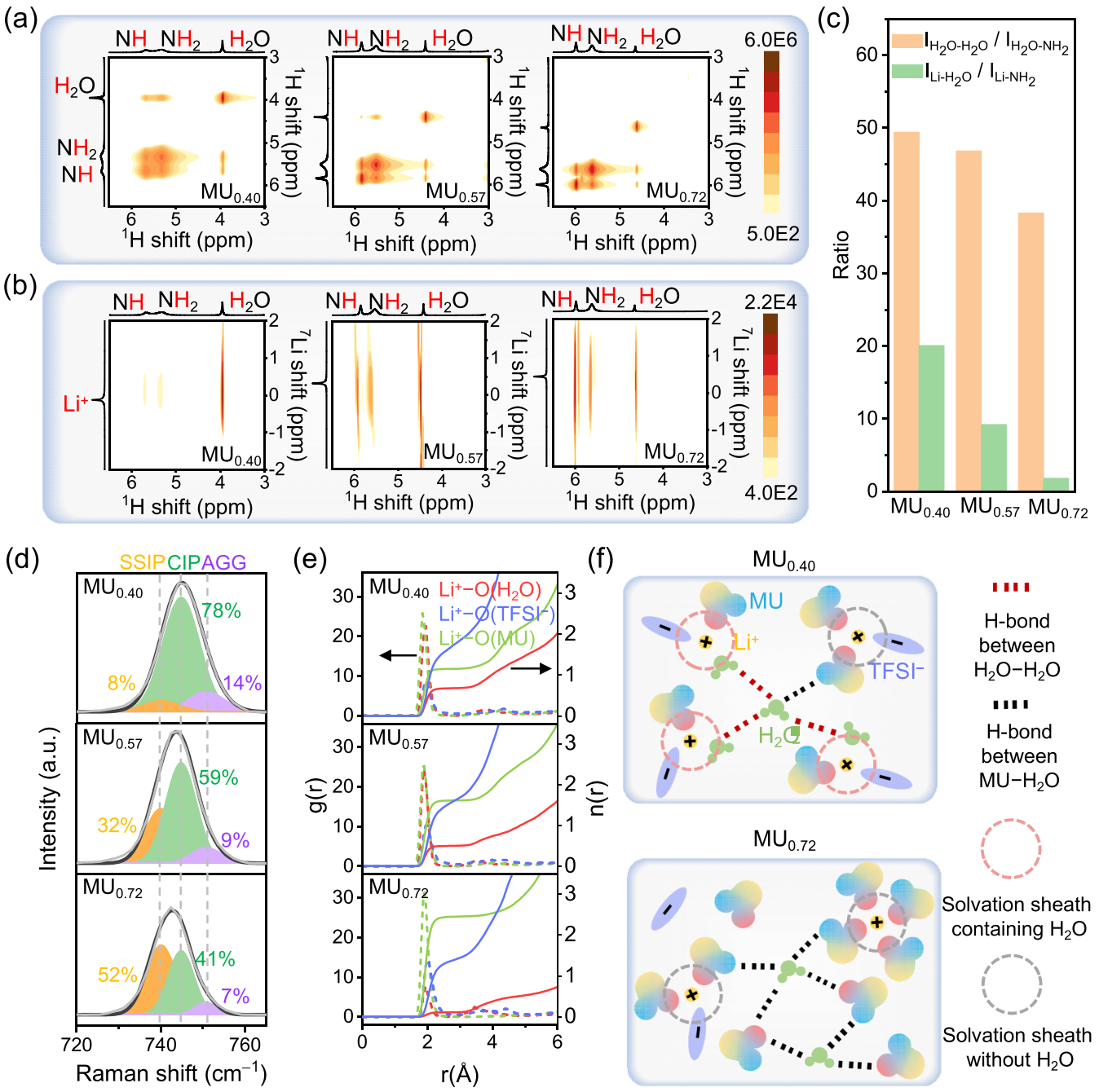

Figure 2. 2D-NMR and AIMD analysis of the solvation structure in MU_x electrolytes. (a) $^1H-^1H$ NOESY and (b) $^7Li-^1H$ HOESY NMR spectra of the MU_x electrolytes. (c) Key NMR cross-peak intensity quantifying the changing molecular interactions in MU_x electrolytes. (d) Raman spectra (S−N−S region) and deconvolution showing the distribution of coordinated $TFSI^-$ anions. (e) Radial distribution function for Li^+−solvent pairs calculated from AIMD simulations. (f) Schematic illustrations of solvation structure in $MU_{0.40}$ and $MU_{0.72}$ electrolytes.

demonstrated the potential of MU, its high salt concentration remained a barrier to practical application. Herein, we shift our electrolyte design from a salt-saturating strategy to a dilute one that leverages the characteristics of structural asymmetry of MU to enhance its miscibility with the LiTFSI salt and water. This approach yields a 2.6 m aqueous electrolyte that not only reduces salt content, viscosity, and density, but also enhances ionic conductivity and broadens the electrochemical stability window to 3.3 V. Unlike conventional 2.6 m aqueous electrolytes dominated by $Li^+(H_2O)_4$ clusters and extensive (H_2O-H_2O) hydrogen bond networks, the solvation sheath of MU-regulated electrolyte is restructured owing to the donor−acceptor amphiphilicity of MU: most H_2O molecules in the inner solvation sheath are replaced by MU and $TFSI^-$, and the excluded H_2O molecules are anchored by MU, converting H_2O-H_2O network into $MU-H_2O$ interactions. This configuration not only reduces the water activity but also promotes the formation of a robust solid electrolyte interphase (SEI), characterized by an organic-rich outer layer and an inorganic-rich inner layer, extending the cathodic stability limit to 1.2 V vs Li^+/Li and enabling compatibility with high-specific-capacity NbO_2 anodes. Under rigorous testing conditions (1.65 mAh cm^{-2}; P/N = 1.2; 0.25 C; conventional aluminum current collector), rocking−chair $NbO_2|LiCoO_2$

https://doi.org/10.1021/acsenergylett.5c03327
ACS Energy Lett. 2026, 11, 654−663

(184 Wh $kg^{-1}_{cathode+anode}$) and NbO_2|$LiMn_2O_4$ (161 Wh $kg^{-1}_{cathode+anode}$) pouch cells exhibited 96% capacity retention after 24 h of storage at 100% state of charge (SOC) and stable cycling over 150 cycles. This simple and effective strategy significantly enhances the energy density of aqueous batteries while retaining advantages such as low cost and safety, advancing the practical development of high-voltage aqueous batteries.

Asymmetric Design Unlocks Dilute Aqueous Electrolytes. Incorporating organic compounds to reconfigure the solution structure is an effective strategy for widening the electrochemical window of aqueous electrolytes and reducing the cost of high-concentration water-in-salt (WIS) electrolytes.[20−22] Among various reported compounds, urea (U) and MU, both containing dual functional groups −C═O and $-NH_2$, have demonstrated strong capabilities to reduce the activity of water molecules and have been introduced into electrolytes to enhance the electrochemical stability of aqueous systems.[19,23] However, electrolytes based on urea face two critical limitations. First, in the previously reported LiTFSI−H_2O−U system, the optimized 4.5 m low-concentration electrolyte exhibits a cathodic stability limit of only 1.5 V vs Li^+/Li, which fails to fully harness the specific capacity advantage of niobium-based oxide anodes. Second, and more critically, urea's physical structure inherently restricts its use in the desired low-salt-concentration regimes. This limitation arises because the high symmetry of urea molecules promotes a tightly packed crystal lattice held by extensive hydrogen bonds. This results in high lattice energy and, consequently, poor solubility, preventing the formation of a homogeneous liquid electrolyte when large proportions of urea are required. In contrast, MU addresses these limitations through a simple yet effective structural modification. The methyl substitution in MU breaks the molecular symmetry. Electrostatic potential (ESP) calculations reveal that the methyl group alters the charge distribution of MU (Figure 1a), disrupting the formation of an ordered MU−MU hydrogen bond network. This leads to looser crystal packing, reduced dissolution energy, and an enhanced ability to solvate cations (Figure 1b). Solubility tests confirmed that the LiTFSI−H_2O−MU system has a broader liquid-phase region (Figure 1c). This superior solubility is the key, as it unlocks a vast and previously inaccessible compositional space, making MU an ideal candidate for developing the desired low-salt-concentration aqueous electrolytes.

By gradually introducing U or MU into ca. 1:1 LiTFSI/H_2O mixtures, we prepared electrolytes with varying concentrations, denoted as U_x or MU_x, where x represents the mole fraction of U or MU in the solution. Compositions such as $U_{0.40}$ and $U_{0.72}$, located outside the liquid−phase region, were immiscible (Figure 1d). In comparison, $MU_{0.40}$, $MU_{0.48}$, $MU_{0.57}$, $MU_{0.65}$, and $MU_{0.72}$ remained homogeneous. Therefore, the MU_x system was selected for further study to allow flexible tuning of the component ratios to optimize physicochemical properties. The compositions and physicochemical properties of different MU_x electrolytes are summarized in Table S1. As shown in Figure 1e, the $MU_{0.40}$ sample has a LiTFSI mole fraction (M_{LiTFSI}) of 0.31, corresponding to a concentration of 8.9 m (mol kg^{-1}). With increasing MU content, both the mole fraction and the concentration of LiTFSI in the solution gradually decrease. At $MU_{0.72}$, M_{LiTFSI} drops by 53% to 0.145, and the salt concentration decreases by 68% to 2.6 m, resulting in a substantial reduction in electrolyte cost compared to conventional salt-concentrated strategy. Interestingly, the gradual incorporation of solid MU does not degrade the electrolyte's physicochemical properties. The $MU_{0.72}$ electrolyte, near the liquid-phase boundary, exhibits optimal values in key parameters such as viscosity (279 mPa·s), conductivity (0.53 mS cm^{-1}), and density (1.37 g cm^{-3}) (Table S1 and Figure 1f). Flash point and self-extinguishing time (SET) are two critical parameters for evaluating electrolyte safety. Due to the nonflammable nature of all components, none of the five MU_x electrolytes exhibited a detectable flash point within the broad temperature range of 25−300 °C. Furthermore, ignition tests conducted on the $MU_{0.72}$ sample demonstrated its nonflammable behavior in a butane−oxygen torch flame, with an SET of 0 s g^{-1} (Figure S1). These results confirm that the MU-modulated hybrid electrolyte retains the inherent nonflammable characteristics of aqueous electrolytes.

Solvation Structure Characterization. Solution structure profoundly affects the physicochemical and electrochemical properties of the electrolytes. We used two-dimensional nuclear magnetic resonance (2D-NMR) spectroscopy to probe real-time molecular interactions and ab initio molecular dynamics (AIMD) simulations to provide a detailed atomistic picture of the solvation environment in the MU_x electrolytes. For the electrolytes of $MU_{0.40}$, $MU_{0.57}$, and $MU_{0.72}$, both $^1H-^1H$ nuclear Overhauser effect spectroscopy (NOESY) and $^1H-^7Li$ heteronuclear Overhauser effect spectroscopy (HOESY) spectra (Figure 2a and Figure 2b) revealed strong cross-peak signals for H_2O-NH/NH_2 and Li^+-NH/NH_2, indicating that MU interacts strongly with both lithium ions and H_2O. As the MU content increases, the ^1H signal of H_2O shifts downfield, which is attributed to the increased formation of H_2O−MU hydrogen bonds, reducing the electron density around the protons of water molecules. This observation is supported by two critical quantitative changes. First, there was a gradual decrease in the ratio of H_2O-H_2O to H_2O-NH_2 cross-peak intensities ($I_{H_2O-H_2O}/I_{H_2O-NH_2}$, Figure 2c), reflecting a reduction in water−water hydrogen bonds and their replacement mainly by H_2O−MU hydrogen bonding. Second, the Li−H_2O to Li−NH_2 cross-peak intensity ratio (I_{Li-H_2O}/I_{Li-NH_2}) also decreases gradually, indicating that continued introduction of MU not only disrupts water−water hydrogen bonds but also displaces water molecules from the solvation sheath. Furthermore, this restructured solvation environment yields another advantage related to anion coordination and the formation of a protective SEI. Raman spectroscopy of the S−N−S bending region (730−760 cm^{-1}, Figure 2d) revealed that even in 2.6 m $MU_{0.72}$ electrolyte, approximately 48% of $TFSI^-$ remains coordinated with Li^+. This high degree of anion coordination would alter the decomposition path of the electrolyte as compared to conventional dilute solution (see discussion below).

These experimental findings are strongly supported by our AIMD simulations, which offer a quantitative atomistic picture of the restructured environment. Radial distribution functions (RDF, g(r)) and coordination numbers (n(r)) were calculated for Li^+-H_2O, Li^+-TFSI^-, and Li^+−MU pairs (Figure 2e), and the inner solvation shell coordination numbers are summarized in Table S2. It is observed that water molecules, MU, and $TFSI^-$ all participate in the primary solvation shell of Li^+. Compared with $MU_{0.40}$ and $MU_{0.57}$, the intensity of the H_2O solvation peak in $MU_{0.72}$ decreases significantly. The coordination number of H_2O within the inner solvation sheath

https://doi.org/10.1021/acsenergylett.5c03327
ACS Energy Lett. 2026, 11, 654−663

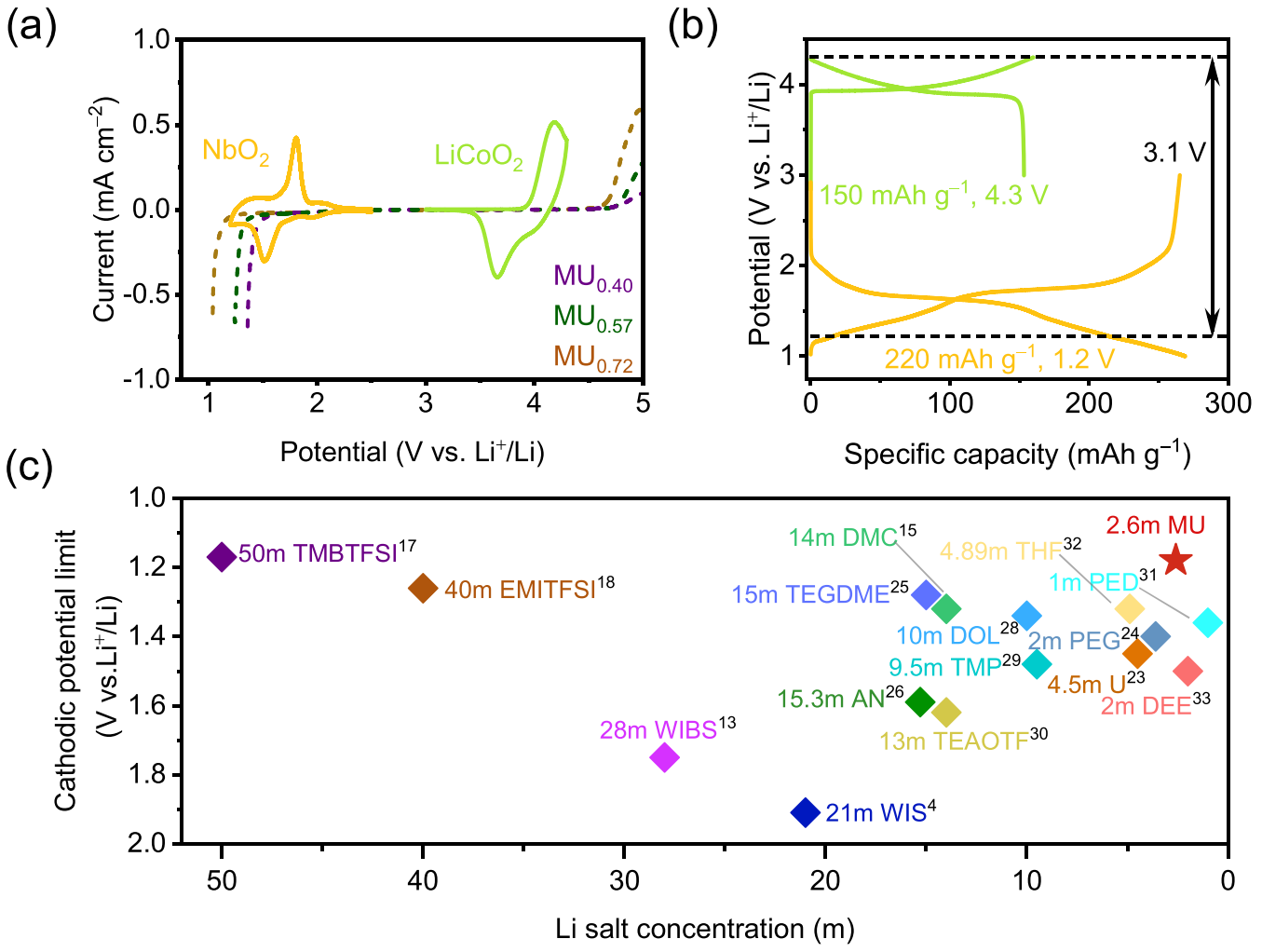

Figure 3. Electrochemical stability window of $MU_{0.72}$ (2.6 m). (a) LSV curves on carbon-coated Al electrode in the MU_x electrolytes, together with CV curves of the NbO_2 and $LiCoO_2$ electrodes. (b) Potential utilization window of the $LiCoO_2$ cathode and NbO_2 anode in $MU_{0.72}$. (c) Comparison of cathodic potential limits and lithium salt concentrations across representative aqueous lithium-ion electrolytes.

(at 2.5 Å) drops from 0.67 to 0.1, while the coordination number of $TFSI^-$ changes only slightly from 1.55 to 1.29. These simulation results are consistent with experimental observations: in $MU_{0.72}$, the primary solvation shell of Li^+ is mainly composed of $TFSI^-$ and MU, with most H_2O molecules surrounding the outer layer and being anchored by the left MU (Figure 2f). Notably, $MU_{0.72}$ (2.6 m) shows a dramatically different solution structure from the conventional 2.6 m LiTFSI/H_2O solution ($MU_{0.00}$) that is dominated by $Li^+(H_2O)_4$ clusters and extensive (H_2O–H_2O) hydrogen-bond networks (see Figure S2 and Table S2). Hence, this redistribution of water molecules in $MU_{0.72}$ leads to disruption of the H_2O–H_2O network and a decrease of water activity, which could benefit an expanded electrochemical stability window of $MU_{0.72}$.

Electrochemical Stability Window. We carried out linear sweep voltammetry (LSV) measurements to evaluate the electrochemical stability window of the as-prepared electrolytes. The carbon-coated Al foil was used as the working electrode instead of bare Ti because the former is more suitable for practical applications and its larger surface area could enlarge the current density.[19,24] As shown in Figure 3a, the electrochemical stability window of the MU_x electrolytes indeed progressively expanded with increasing MU content, reaching up to 3.3 V (1.2–4.5 V vs Li^+/Li) for $MU_{0.72}$. This enhancement was accompanied by a downward shift in the cathodic onset potential, from 1.6 V in $MU_{0.40}$ to 1.2 V in $MU_{0.72}$ vs Li^+/Li (Figure 3a). Characteristic peaks in the cyclic voltammetry (CV) data further confirmed that the $MU_{0.72}$ electrolyte supports reversible lithium insertion and extraction in both NbO_2 and $LiCoO_2$ electrodes. Accordingly, a full rocking-chair lithium-ion cell using NbO_2 as the anode and $LiCoO_2$ as the cathode could achieve a high cutoff voltage of 3.1 V and a high theoretical energy density of approximately 200 Wh $kg^{-1}_{cathode+anode}$ (Figure 3b). To enable a direct comparison with previously reported representative aqueous electrolytes, we performed LSV measurements on those electrolytes under identical conditions (Figure S3). Notably, $MU_{0.72}$ demonstrated a lower cathodic limit than most reported aqueous electrolytes based on salt-concentrated or water–organic hybrid strategies.[4,13,15,17,23−33] Its performance even approached that of ultrahigh-concentration lithium salt–ionic liquid electrolyte (e.g., 50 m LiTFSI + 30 m TMBTFSI in H_2O) (Figure 3c), while using significantly less lithium salt. Therefore, compared with previous reports utilizing niobium-based oxides as anodes, our approach offers multiple advantages, including a lower lithiation potential, higher

https://doi.org/10.1021/acsenergylett.5c03327
ACS Energy Lett. 2026, 11, 654−663

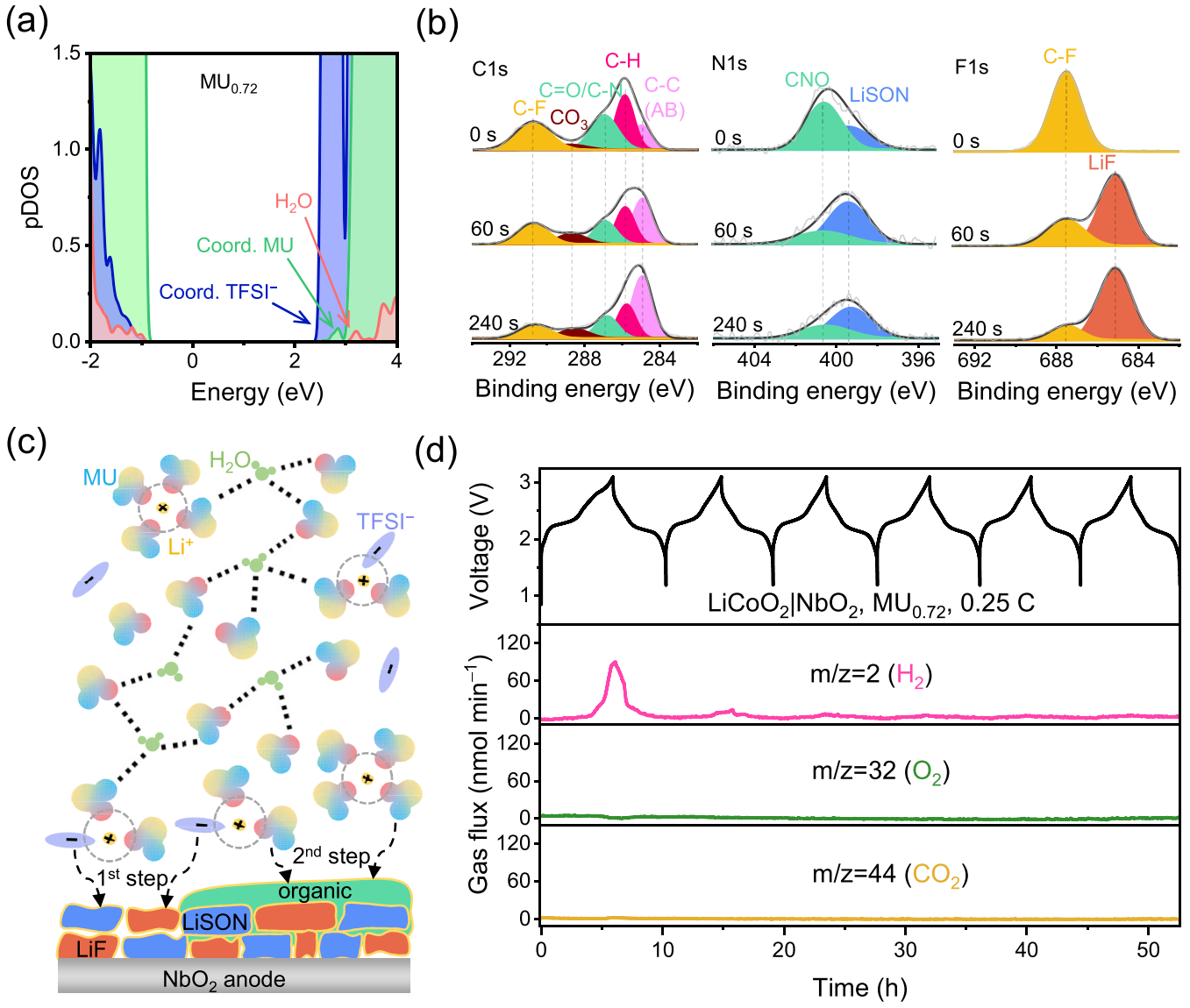

Figure 4. Understanding and characterization of $MU_{0.72}$ derived SEI. (a) Calculated pDOS for the $MU_{0.72}$ electrolyte components, predicting that $TFSI^-$ anions and MU molecules will be preferentially reduced over water. (b) XPS depth-profiling of the NbO_2 anode after cycling. The spectra confirm the formation of a dual-layer SEI with an inorganic-rich inner layer and an organic-rich outer layer. AB stands for acetylene black. (c) Schematic illustration of the SEI formation on the NbO_2 anode surface. The initially preferential reduction of $TFSI^-$ leads to the formation of the inorganic-rich inner layer, while the subsequent reduction of MU results in the formation of the organic-rich outer layer. (d) In-situ DEMS analysis of the $LiCoO_2|NbO_2$ full cell using the $MU_{0.72}$ electrolyte during cycling.

specific capacity, and substantially reduced salt concentration (Table S3).

Interphase Formation and Characterization. The electrochemical stability window of electrolyte is widely reported to be associated with either the solution structure[24,31] or the SEI[34] or both.[4,21,23,32] To understand the broadened electrochemical stability window of $MU_{0.72}$, we investigated the lowest unoccupied molecular orbital (LUMO) based on its solution structure and characterized the composition and configuration of its derived SEI. The projected density of states (pDOS) for the 2.6 m low-concentration $MU_{0.72}$ electrolyte is shown in Figure 4a and Figure S4. The LUMO of the solution is primarily composed of contributions from $TFSI^-$, followed by contributions from MU and H_2O at progressively higher energy levels. This energy alignment suggests that during reduction $TFSI^-$ and MU will decompose preferentially over H_2O. As a result, H_2O remains reductively stable, while the decomposition of $TFSI^-$ and MU generates passivation products that further prevent the electrolyte from decomposition on the NbO_2 surface, both of which contribute to the broader electrochemical stability window observed in $MU_{0.72}$.

To investigate the SEI on the NbO_2 anode, we conducted X-ray photoelectron spectroscopy (XPS) analysis. As shown in Figure 4b, the spectra reveal the presence of MU-derived organic species (C−H, C−N, and C═O in the C 1s region; CNO in N 1s), and $TFSI^-$-derived inorganic species such as LiF and lithium sulfur oxynitride (LiSON). With progressive Ar^+ sputtering, the intensities of the CNO and C−H species decrease, while the signals for LiF and LiSON become significantly more prominent. These depth-dependent changes indicate that, despite the low lithium salt concentration, the high degree of $TFSI^-$ and MU coordination in the solvation structure of $MU_{0.72}$ promotes successive decomposition of $TFSI^-$ and MU to form a dual-layered SEI that is organically

https://doi.org/10.1021/acsenergylett.5c03327
ACS Energy Lett. 2026, 11, 654−663

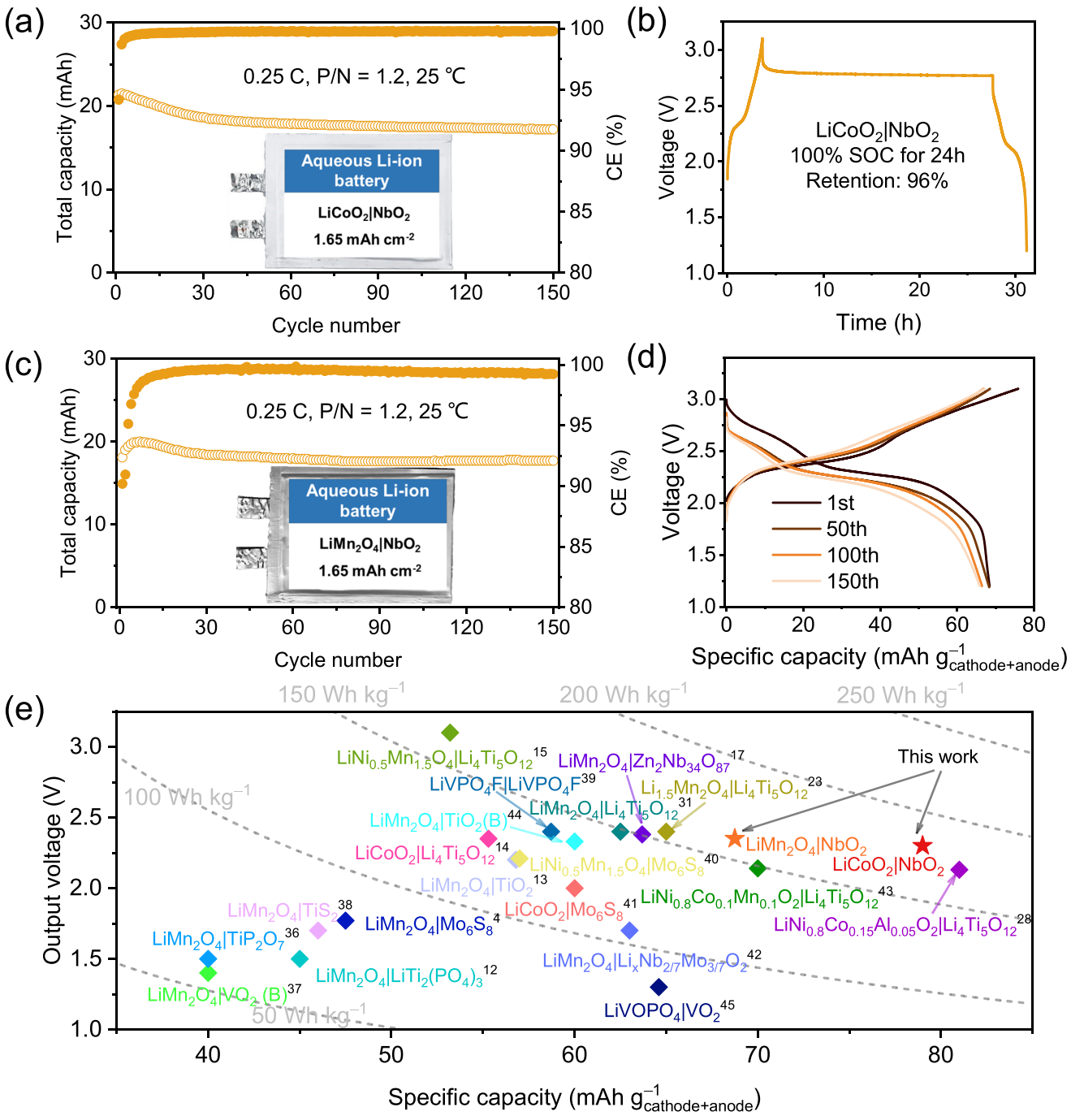

Figure 5. Electrochemical performances of aqueous pouch cells using NbO_2 anode and $MU_{0.72}$ electrolyte. (a) Cycling performance and (b) self-discharge behavior of the $LiCoO_2|NbO_2$ pouch cell. (c) Cycling performance and (d) charge−discharge profiles of the $LiMn_2O_4|NbO_2$ pouch cell. (e) Comparison of energy density for representative aqueous lithium-ion batteries.

rich on the surface and inorganic-rich beneath. This SEI formation is schematically illustrated in Figure 4c, consistent with the simulation results, as shown in Figure 4a.

In-situ differential electrochemical mass spectrometry measurement (DEMS) was further employed to monitor gaseous products during full-cell operation, providing direct evidence of the SEI's effectiveness in suppressing side reactions between the electrolyte and electrodes. As shown in Figure 4d, no significant O_2 or CO_2 signals were detected throughout the entire testing process. In contrast, a significant H_2 signal emerged during the first charge cycle when the voltage exceeded over 2.7 V. However, in the second cycle, the H_2 signal intensity decreased dramatically, and from the third to sixth cycles, no detectable gas evolution was observed. Combining the results from both mass spectrometry and XPS, it is deduced that the initial formation of $TFSI^-$-derived inorganic-rich SEI is insufficient to suppress the hydrogen evolution reaction (HER) completely; the following addition of MU-derived organic-rich SEI may become necessary to compact the SEI and prevent HER more efficiently. These findings highlight that SEI engineering through solvation structure design is as crucial as water activity modulation. The combined effect of low water activity and a robust SEI provides

https://doi.org/10.1021/acsenergylett.5c03327
ACS Energy Lett. 2026, 11, 654−663

synergistic thermodynamic and kinetic suppression of the HER.

High-Energy-Density Aqueous Pouch Cells. The aforementioned results clearly demonstrate that the $MU_{0.72}$ aqueous electrolyte, with a low salt concentration of 2.6 m, significantly extends the cathodic stability limit to 1.2 V vs Li^+/Li, with HER effectively suppressed during cycling. To evaluate the long-term cycling compatibility of the as-prepared MU_x electrolytes with the NbO_2 anode under practical conditions, we assembled $LiCoO_2|NbO_2$ pouch cells using 3.5 × 4.7 cm $LiCoO_2$ cathodes (~12.0 mg cm^{-2}) and NbO_2 anodes (~6.7 mg cm^{-2}), both supported on aluminum current collectors. The positive-to-negative electrode capacity ratio (P/N) was maintained at ~1.2. The pouch cells were fabricated in an ambient atmosphere without moisture control.

As shown in Figure 5a and Figure S5, under stringent testing conditions of a small rate of 0.25 C, the $LiCoO_2|NbO_2$ pouch cell employing the $MU_{0.72}$ electrolyte delivered a high initial Coulombic efficiency of ~ 93% and a reversible capacity of ~ 79 mAh $g^{-1}_{cathode+anode}$ (based on the total mass of cathode and anode materials). The cell retained 80% of its initial capacity after 150 cycles, with an average Coulombic efficiency of 99.8%, demonstrating excellent cycling stability. Furthermore, this battery exhibited strong self-discharge resistance (Figure 5b), retaining 96% of its capacity after 24 h at 100% SOC, confirming the minimal occurrence of side reactions under these harsh conditions. In contrast, cells using $MU_{0.40}$ and $MU_{0.57}$ electrolytes showed significantly lower initial Coulombic efficiencies of 55.8% and 78.9%, respectively, and their capacities dropped below 70% within the first 10 cycles, indicating poor compatibility with the low-potential NbO_2 anode (Figure S5).

Considering the low cost and stable spinel structure of $LiMn_2O_4$, we further assembled $LiMn_2O_4|NbO_2$ pouch cells for comparison. As shown in Figures 5c and 5d, the $MU_{0.72}$-based $LiMn_2O_4|NbO_2$ cell exhibited a high capacity retention of 88.5% over 150 cycles at 0.25 C, further confirming the robustness of the $MU_{0.72}$ electrolyte across different battery chemistries. In terms of energy density, our fabricated $LiCoO_2|NbO_2$ and $LiMn_2O_4|NbO_2$ pouch cells achieved gravimetric energy densities of ~184 and ~161 Wh $kg^{-1}_{cathode+anode}$, respectively, outperforming previously reported aqueous batteries[4,12,14,35−45] (Figure 5e and Table S4). Importantly, these results were achieved using a 2.6 m MU-modulated aqueous electrolyte without compromising cost-effectiveness or safety, underscoring the potential of our electrolyte design for practical applications in high-voltage aqueous lithium-ion batteries.

In summary, we present a simple yet effective diluting electrolyte strategy for the development of high-voltage aqueous batteries. By leveraging the structural asymmetry of MU, we accessed a previously unexplored compositional space of low-salt concentration LiTFSI−H_2O−MU electrolytes, which is inaccessible for the LiTFSI−H_2O−U electrolytes using symmetric urea. Within this uncharted regime, the solvation structure can be further tuned by adjusting the MU content, taking advantage of its donor−acceptor amphiphilicity. This property enables simultaneous modulation of the inner solvation sheath and anchoring of water molecules in the outer coordination layer. As a result, we developed a 2.6 m aqueous electrolyte with suppressed water activity and the ability to form a stable organic−inorganic dual-layer interphase. This interphase effectively mitigates parasitic hydrogen evolution, extending the cathodic stability limit to 1.2 V vs Li^+/Li and enabling compatibility with low-potential, high-capacity NbO_2 anode. Under stringent testing conditions (P/N ratio = 1.2; Al current collectors), $NbO_2|LiCoO_2$ (184 Wh $kg^{-1}_{cathode+anode}$) and $NbO_2|LiMn_2O_4$ (161 Wh $kg^{-1}_{cathode+anode}$) pouch cells demonstrated 96% capacity retention after 24 h at 100% SOC and stable cycling over 150 cycles, even at a low rate of 0.25 C. This diluting electrolyte strategy reduces salt concentration, viscosity, and density while simultaneously enhancing ionic conductivity and broadening the electrochemical stability window. Consequently, it significantly enhances the energy density of aqueous batteries without compromising cost-effectiveness or safety, thereby promoting their practical advancement.

■ ASSOCIATED CONTENT

Supporting Information

The Supporting Information is available free of charge at https://pubs.acs.org/doi/10.1021/acsenergylett.5c03327.

Experimental methods regarding electrolyte and electrode preparation, CV, LSV, Raman, 2D-NMR, ionic conductivity and viscosity measurements for electrolytes, XPS, in-suit DEMS measurements, and computational details (PDF)

■ AUTHOR INFORMATION

Corresponding Authors

Shi Liu − *Research Center for Industries of the Future and Department of Physics, School of Science, Westlake University, Hangzhou 310030, China; Institute of Natural Sciences, Westlake Institute for Advanced Study, Hangzhou 310024, China;* orcid.org/0000-0002-8488-4848; Email: liushi@westlake.edu.cn

Jianhui Wang − *Division of Solar Energy Conversion and Catalysis at Westlake University, Zhejiang Baima Lake laboratory Co. Ltd., Hangzhou 310000, China; Zhejiang Key Laboratory of 3D Micro/Nano Fabrication and Characterization, Department of Electronic and Information Engineering, School of Engineering and Research Center for Industries of the Future, Westlake University, Hangzhou 310030, China; Institute of Advanced Technology, Westlake Institute for Advanced Study, Hangzhou 310024, China;* orcid.org/0000-0002-4170-1132; Email: wangjianhui@westlake.edu.cn

Authors

Chuanyu Hou − *School of Materials Science & Engineering, Zhejiang University, Hangzhou 310024 Zhejiang, China; Zhejiang Key Laboratory of 3D Micro/Nano Fabrication and Characterization, Department of Electronic and Information Engineering, School of Engineering and Research Center for Industries of the Future, Westlake University, Hangzhou 310030, China; Institute of Advanced Technology, Westlake Institute for Advanced Study, Hangzhou 310024, China*

Changming Ke − *Department of Physics, School of Science, Westlake University, Hangzhou 310030, China; Institute of Natural Sciences, Westlake Institute for Advanced Study, Hangzhou 310024, China*

Runze Chen − *School of Materials Science & Engineering, Zhejiang University, Hangzhou 310024 Zhejiang, China; Zhejiang Key Laboratory of 3D Micro/Nano Fabrication*

https://doi.org/10.1021/acsenergylett.5c03327
ACS Energy Lett. 2026, 11, 654−663

and Characterization, Department of Electronic and Information Engineering, School of Engineering and Research Center for Industries of the Future, Westlake University, Hangzhou 310030, China; Institute of Advanced Technology, Westlake Institute for Advanced Study, Hangzhou 310024, China

Yangfan Lin − *Zhejiang Key Laboratory of 3D Micro/Nano Fabrication and Characterization, Department of Electronic and Information Engineering, School of Engineering and Research Center for Industries of the Future, Westlake University, Hangzhou 310030, China; Institute of Advanced Technology, Westlake Institute for Advanced Study, Hangzhou 310024, China;* orcid.org/0000-0003-2297-4124

Qin Huang − *Zhejiang Key Laboratory of 3D Micro/Nano Fabrication and Characterization, Department of Electronic and Information Engineering, School of Engineering and Research Center for Industries of the Future, Westlake University, Hangzhou 310030, China; Institute of Advanced Technology, Westlake Institute for Advanced Study, Hangzhou 310024, China*

Complete contact information is available at: https://pubs.acs.org/10.1021/acsenergylett.5c03327

Author Contributions

J.W. and C.H. designed the experiments. C.H. carried out electrolyte preparation, solution structure characterizations and electrochemical performances. C.K. and S.L. designed and performed the AIMD simulations. All authors contributed to the data analysis and manuscript preparation. J.W. conceived and led the project. C.H. and C.K. contributed equally to this work.

Notes

The authors declare no competing financial interest.

■ ACKNOWLEDGMENTS

This work was supported by Zhejiang Baima Lake Laboratory Co. Ltd., Zhejiang Key Laboratory of 3D Micro/Nano Fabrication and Characterization, Research Center for Industries of the Future (RCIF), Westlake Education Foundation, National Natural Science Foundation of China (Grant No. 21975207) and Zhejiang Provincial Natural Science Foundation of China (LR25A040004). The computational resource is provided by the Open Source Supercomputing Center of S-A-I.

■ REFERENCES

(1) Armand, M.; Tarascon, J. M. Building Better Batteries. *Nature* **2008**, *451* (7179), 652−657.

(2) Xu, K. Nonaqueous Liquid Electrolytes for Lithium-Based Rechargeable Batteries. *Chem. Rev.* **2004**, *104* (10), 4303−4418.

(3) Yamada, Y.; Wang, J.; Ko, S.; Watanabe, E.; Yamada, A. Advances and Issues in Developing Salt-Concentrated Battery Electrolytes. *Nat. Energy* **2019**, *4* (4), 269−280.

(4) Suo, L.; Borodin, O.; Gao, T.; Olguin, M.; Ho, J.; Fan, X.; Luo, C.; Wang, C.; Xu, K. "Water-in-salt" Electrolyte Enables High-Voltage Aqueous Lithium-ion Chemistries. *Science* **2015**, *350* (6263), 938−943.

(5) Kim, H.; Hong, J.; Park, K.-Y.; Kim, H.; Kim, S.-W.; Kang, K. Aqueous Rechargeable Li and Na Ion Batteries. *Chem. Rev.* **2014**, *114* (23), 11788−11827.

(6) Liang, G.; Mo, F.; Ji, X.; Zhi, C. Non-metallic Charge Carriers for Aqueous Batteries. *Nat. Rev. Mater.* **2021**, *6* (2), 109−123.

(7) Zhang, F.; Zhang, W.; Wexler, D.; Guo, Z. Recent Progress and Future Advances on Aqueous Monovalent-Ion Batteries towards Safe and High-Power Energy Storage. *Adv. Mater.* **2022**, *34* (24), No. 2107965.

(8) Liang, Y.; Yao, Y. Designing Modern Aqueous Natteries. *Nat. Rev. Mater.* **2023**, *8* (2), 109−122.

(9) Zhang, H.; Liu, X.; Li, H.; Hasa, I.; Passerini, S. Challenges and Strategies for High-Energy Aqueous Electrolyte Rechargeable Batteries. *Angew. Chem., Int. Ed.* **2021**, *60* (2), 598−616.

(10) Griffith, K. J.; Wiaderek, K. M.; Cibin, G.; Marbella, L. E.; Grey, C. P. Niobium Tungsten Oxides for High-Rate Lithium-Ion Energy Storage. *Nature* **2018**, *559* (7715), 556−563.

(11) Yang, Y.; Zhao, J. Wadsley−Roth Crystallographic Shear Structure Niobium-Based Oxides: Promising Anode Materials for High-Safety Lithium-Ion Batteries. *Adv. Sci.* **2021**, *8* (12), No. 2004855.

(12) Luo, J.-Y.; Cui, W.-J.; He, P.; Xia, Y.-Y. Raising the Cycling Stability of Aqueous Lithium-Ion Batteries by Eliminating Oxygen in the Electrolyte. *Nat. Chem.* **2010**, *2* (9), 760−765.

(13) Suo, L.; Borodin, O.; Sun, W.; Fan, X.; Yang, C.; Wang, F.; Gao, T.; Ma, Z.; Schroeder, M.; von Cresce, A.; et al. Advanced High-Voltage Aqueous Lithium-Ion Battery Enabled by "Water-in-Bisalt" Electrolyte. *Angew. Chem., Int. Ed.* **2016**, *55* (25), 7136−7141.

(14) Yamada, Y.; Usui, K.; Sodeyama, K.; Ko, S.; Tateyama, Y.; Yamada, A. Hydrate-Melt Electrolytes for High-Energy-Density Aqueous Batteries. *Nat. Energy* **2016**, *1* (10), No. 16129.

(15) Wang, F.; Borodin, O.; Ding, M. S.; Gobet, M.; Vatamanu, J.; Fan, X.; Gao, T.; Eidson, N.; Liang, Y.; Sun, W.; et al. Hybrid Aqueous/Non-aqueous Electrolyte for Safe and High-Energy Li-Ion Batteries. *Joule* **2018**, *2* (5), 927−937.

(16) Lakhnot, A. S.; Gupta, T.; Singh, Y.; Hundekar, P.; Jain, R.; Han, F.; Koratkar, N. Aqueous Lithium-Ion Batteries with Niobium Tungsten Oxide Anodes for Superior Volumetric and Rate Capability. *Energy Storage Mater.* **2020**, *27*, 506−513.

(17) Zhu, X.; Mao, M.; Lin, Z.; Yue, J.; Li, M.; Lv, T.; Zhou, A.; Hu, Y.-S.; Li, H.; Huang, X.; et al. Wadsley-Roth Phase Niobium-Based Oxide Anode Promising High Power and Energy Density Aqueous Li-Ion Batteries. *ACS Mater. Lett.* **2022**, *4*, 1574−1583.

(18) Becker, M.; Bernasconi, F.; Egorov, K.; Svaluto-Ferro, E.; Kühnel, R.-S.; Battaglia, C. J. E. S. M. Niobium Oxide Anode Materials with Suppressed Activity Toward Hydrogen Evolution Reaction for Aqueous Batteries. *Energy Storage Mater.* **2024**, *71*, No. 103613.

(19) Lin, R.; Ke, C.; Chen, J.; Liu, S.; Wang, J. Asymmetric Donor-Acceptor Molecule-Regulated Core-Shell-Solvation Electrolyte for High-Voltage Aqueous Batteries. *Joule* **2022**, *6* (2), 399−417.

(20) Zhou, L.; Tian, S.; Du, X.; Liu, T.; Zhang, H.; Zhang, J.; Hu, S.; Chen, Z.; Zhang, J.; Cui, G. Suppressing Hydrogen Evolution in Aqueous Lithium-Ion Batteries with Double-Site Hydrogen Bonding. *ACS Energy Lett.* **2023**, *8* (1), 40−47.

(21) Jeong, I.; Kim, S.; Kim, Y.; Kim, C.; Kang, J.; Ha, J. H.; Cho, Y.; Kang, S. J.; Ryu, J.; Han, J. W.; et al. Toward Long-Life High-Voltage Aqueous Li-Ion Batteries: from Solvation Chemistry to Solid-Electrolyte-Interphase Layer Optimization Against Electron Tunneling Effect. *Adv. Mater.* **2025**, *37* (6), No. 2412652.

(22) Shang, Y.; Chen, N.; Li, Y.; Chen, S.; Li, Z.; Li, S.; Ren, X.; Ye, Y.; Li, L.; Wu, F.; et al. Tiny-Ligand Solvation Electrolyte Enabled Fast-Charging Aqueous Batteries. *Angew. Chem., Int. Ed.* **2025**, *64* (14), No. e202423808.

(23) Xu, J.; Ji, X.; Zhang, J.; Yang, C.; Wang, P.; Liu, S.; Ludwig, K.; Chen, F.; Kofinas, P.; Wang, C. Aqueous Electrolyte Design for Super-Stable 2.5 V $LiMn_2O_4$ ‖ $Li_4Ti_5O_{12}$ Pouch Cells. *Nat. Energy* **2022**, *7* (2), 186−193.

(24) Xie, J.; Liang, Z.; Lu, Y. C. Molecular Crowding Electrolytes for High-Voltage Aqueous Batteries. *Nat. Mater.* **2020**, *19* (9), 1006−1011.

(25) Shang, Y.; Chen, N.; Li, Y.; Chen, S.; Lai, J.; Huang, Y.; Qu, W.; Wu, F.; Chen, R. An "Ether-In-Water" Electrolyte Boosts Stable

Interfacial Chemistry for Aqueous Lithium-Ion Batteries. *Adv. Mater.* **2020**, *32* (40), No. 2004017.
(26) Chen, J.; Vatamanu, J.; Xing, L.; Borodin, O.; Chen, H.; Guan, X.; Liu, X.; Xu, K.; Li, W. Improving Electrochemical Stability and Low-Temperature Performance with Water/Acetonitrile Hybrid Electrolytes. *Adv. Energy Mater.* **2020**, *10* (3), No. 1902654.
(27) Becker, M.; Rentsch, D.; Reber, D.; Aribia, A.; Battaglia, C.; Kühnel, R.-S. The Hydrotropic Effect of Ionic Liquids in Water-in-Salt Electrolytes. *Angew. Chem., Int. Ed.* **2021**, *60* (25), 14100−14108.
(28) Ma, Z.; Chen, J.; Vatamanu, J.; Borodin, O.; Bedrov, D.; Zhou, X.; Zhang, W.; Li, W.; Xu, K.; Xing, L. Expanding the Low-Temperature and High-Voltage Limits of Aqueous Lithium-Ion Battery. *Energy Storage Mater.* **2022**, *45*, 903−910.
(29) Li, Q.; Yang, C.; Zhang, J.; Ji, X.; Xu, J.; He, X.; Chen, L.; Hou, S.; Uddin, J.; Addison, D.; et al. Controlling Intermolecular Interaction and Interphase Chemistry Enabled Sustainable Water-tolerance $LiMn_2O_4||Li_4Ti_5O_{12}$ Batteries. *Angew. Chem., Int. Ed.* **2022**, *61* (49), No. e202214126.
(30) Zhou, A.; Zhang, J.; Chen, M.; Yue, J.; Lv, T.; Liu, B.; Zhu, X.; Qin, K.; Feng, G.; Suo, L. An Electric-Field-Reinforced Hydrophobic Cationic Sieve Lowers the Concentration Threshold of Water-In-Salt Electrolytes. *Adv. Mater.* **2022**, *34* (47), No. 2207040.
(31) Lin, R.; Chen, J.; Ke, C.; Liu, S.; Wang, J. A Dilute Fluorine-Free Electrolyte Design for High-Voltage Hybrid Aqueous Batteries. *J. Energy Chem.* **2023**, *77*, 180−190.
(32) Zhang, C.; Chen, B.; Chen, Q.; Liu, Y.; Kong, X.; Suo, L.; Lu, J.; Pan, H. Regulation of Molecular Microheterogeneity in Electrolytes Enables Ampere-Hour-Level Aqueous $LiMn_2O_4||Li_4Ti_5O_{12}$ Pouch Cells. *Adv. Mater.* **2024**, *36* (40), No. 2405913.
(33) Zhang, C.; Chen, B.; Chen, Q.; Tian, C.; Zhou, M.; Zhao, X.; Li, Z.; Fan, L.; Kong, X.; Pan, H. Microstructure Design of Electrolytes for High-Energy-Density Aqueous Batteries. *ACS Energy Lett.* **2024**, *9* (9), 4691−4698.
(34) Zhu, X.; Lin, Z.; Lai, J.; Lv, T.; Lin, T.; Pan, H.; Feng, J.; Wang, Q.; Han, S.; Chen, R.; et al. Highly Efficient Spatially-Temporally Synchronized Construction of Robust Li_3PO_4-rich Solid-Electrolyte Interphases in Aqueous Li-ion Batteries. *Angew. Chem., Int. Ed.* **2024**, *63* (5), No. e202317549.
(35) Suo, L.; Borodin, O.; Sun, W.; Fan, X.; Yang, C.; Wang, F.; Gao, T.; Ma, Z.; Schroeder, M.; von Cresce, A.; et al. Advanced High-Voltage Aqueous Lithium-Ion Battery Enabled by "Water-in-Bisalt" Electrolyte. *Angew. Chem., Int. Ed.* **2016**, *55* (25), 7136−7141.
(36) Wen, Y.; Chen, L.; Pang, Y.; Guo, Z.; Bin, D.; Wang, Y.-g.; Wang, C.; Xia, Y. TiP_2O_7 and Expanded Graphite Nanocomposite as Anode Material for Aqueous Lithium-Ion Batteries. *ACS Appl. Mater.* **2017**, *9* (9), 8075−8082.
(37) Ni, J.; Jiang, W.; Yu, K.; Gao, Y.; Zhu, Z. Hydrothermal synthesis of VO_2 (B) Nanostructures and Application in Aqueous Li-Ion Battery. *Electrochim. Acta* **2011**, *56* (5), 2122−2126.
(38) Sun, W.; Suo, L.; Wang, F.; Eidson, N.; Yang, C.; Han, F.; Ma, Z.; Gao, T.; Zhu, M.; Wang, C. "Water-in-Salt" Electrolyte Enabled $LiMn_2O_4/TiS_2$ Lithium-Ion Batteries. *Electrochem. Commun.* **2017**, *82*, 71−74.
(39) Yang, C.; Ji, X.; Fan, X.; Gao, T.; Suo, L.; Wang, F.; Sun, W.; Chen, J.; Chen, L.; Han, F.; et al. Flexible Aqueous Li-Ion Battery with High Energy and Power Densities. *Adv. Mater.* **2017**, *29* (44), No. 1701972.
(40) Wang, F.; Suo, L.; Liang, Y.; Yang, C.; Han, F.; Gao, T.; Sun, W.; Wang, C. Spinel $LiNi_{0.5}Mn_{1.5}O_4$ Cathode for High-Energy Aqueous Lithium-Ion Batteries. *Adv. Energy Mater.* **2017**, *7* (8), No. 1600922.
(41) Wang, F.; Lin, Y.; Suo, L.; Fan, X.; Gao, T.; Yang, C.; Han, F.; Qi, Y.; Xu, K.; Wang, C. Stabilizing High Voltage $LiCoO_2$ Cathode in Aqueous Electrolyte with Interphase-Forming Additive. *Energy Environ. Sci.* **2016**, *9* (12), 3666−3673.
(42) Yun, J.; Sagehashi, R.; Sato, Y.; Masuda, T.; Hoshino, S.; Rajendra, H. B.; Okuno, K.; Hosoe, A.; Bandarenka, A. S.; Yabuuchi, N. Nanosized and Metastable Molybdenum Oxides as Negative Electrode Materials for Durable High-Energy Aqueous Li-Ion Batteries. *Proc. Natl. Acad. Sci. U. S. A.* **2021**, *118* (48), No. e2024969118.
(43) Reber, D.; Borodin, O.; Becker, M.; Rentsch, D.; Thienenkamp, J. H.; Grissa, R.; Zhao, W.; Aribia, A.; Brunklaus, G.; Battaglia, C.; et al. Water/Ionic Liquid/Succinonitrile Hybrid Electrolytes for Aqueous Batteries. *Adv. Funct. Mater.* **2022**, *32* (20), No. 2112138.
(44) Zhou, A.; Liu, Y.; Zhu, X.; Li, X.; Yue, J.; Ma, X.; Gu, L.; Hu, Y.-S.; Li, H.; Huang, X.; et al. TiO_2 (B) Anode for High-Voltage Aqueous Li-Ion Batteries. *Energy Storage Mater.* **2021**, *42*, 438−444.
(45) Shao, M.; Deng, J.; Zhong, F.; Cao, Y.; Ai, X.; Qian, J.; Yang, H. An All-Vanadium Aqueous Lithium Ion Battery with High Energy Density and Long Lifespan. *Energy Storage Mater.* **2019**, *18*, 92−99.

https://doi.org/10.1021/acsenergylett.5c03327
ACS Energy Lett. 2026, 11, 654−663